

## 6 Integrated properties

### 6.1 Luminosities

The Luminosity function  $\Phi(L)$  is the number of galaxies per unit volume per unit luminosity interval (see Binggeli, Sandage & Tammann 1988 for a review). The number of galaxies with luminosity in the range  $(L, L + dL)$  is  $\Phi(L)dL$ . Equivalently, the number of galaxies per unit volume with absolute magnitude in the range  $(M, M + dM)$  is  $\Phi_M(M)dM$ . Since the two must be equal, we have

$$\begin{aligned}\Phi_M(M) &= \Phi(L) \left| \frac{dM}{dL} \right|^{-1}, \\ &= 0.921L\Phi(L)\end{aligned}\tag{6.1}$$

where the constant is more precisely  $0.4 \ln(10)$ .

A convenient empirical fitting formula is that of Schechter (1976)

$$\Phi(x) = \Phi_0 x^\alpha e^{-x}, \quad x \equiv L/L^*.\tag{6.2}$$

The Schechter function has three free parameters,

$\Phi_0$  – characteristic number density

$L^*$  – characteristic luminosity

$\alpha$  – slope parameter

The number density of galaxies with luminosity  $L$  or greater is

$$\begin{aligned}n(L) &= \int_L^\infty \Phi(L)dL, \\ &= \Phi_0 \int_{L/L^*}^\infty x^\alpha e^{-x} dx, \\ &= \Phi_0 \Gamma(\alpha + 1, L/L^*).\end{aligned}\tag{6.3}$$

The luminosity density of galaxies with luminosity  $L$  or greater is

$$\begin{aligned}\rho_L(L) &= \int_L^\infty \Phi(L)LdL, \\ &= \Phi_0 \int_{L/L^*}^\infty x^{\alpha+1} e^{-x} dx, \\ &= \Phi_0 \Gamma(\alpha + 2, L/L^*).\end{aligned}\tag{6.4}$$

Note that  $n(L)$  diverges at low luminosity if  $\alpha \leq -1$ , and  $\rho_L(L)$  diverges at low luminosity if  $\alpha \leq -2$ .

For the overall population one finds  $M_{BT}^* = -20.3 \pm 0.7$ ,  $L_B^* \simeq 2.0 \times 10^{10} L_{B\odot}$ ,  $a \simeq -1.25$ ,  $\Phi_0 \simeq 0.004 \text{ Mpc}^{-3}$ . From this one concludes that the mean blue luminosity density of the Universe is  $\rho_{LB} = (1.1 \pm 0.1) \times 10^8 L_{B\odot} \text{ Mpc}^{-3}$ .

Different morphological types have different luminosity functions (Figure 6.1)

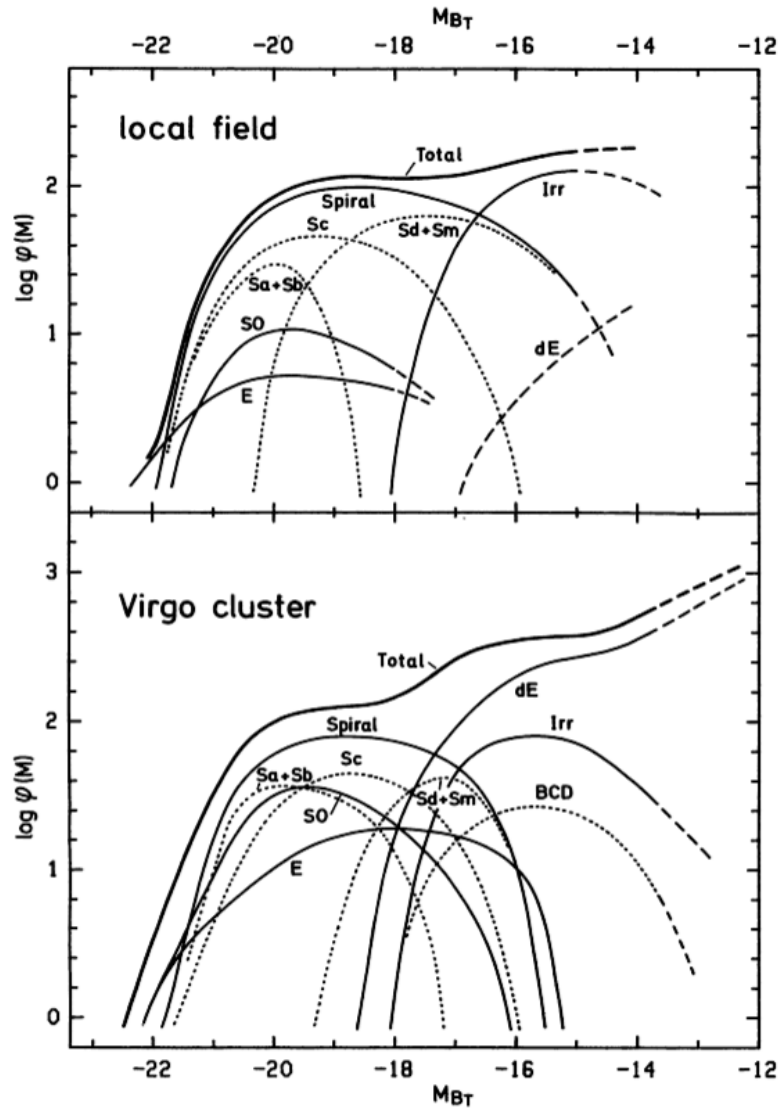


Figure 6.1: Luminosity functions for individual morphological types in field and cluster environments (from Binggeli, Sandage & Tammann 1988).

## 6.2 Diameters

Galaxies do not have distinct diameters. Several definitions have been suggested. The *Holmberg radius* is the length of the semimajor axis of the  $\mu_{pg} = 26.5$  isophote. The *de Vaucouleurs radius* is the radius that the  $\mu_{pg} = 25.0$  isophote would have if the galaxy were seen face on and unobscured by dust.

The *standard diameter* ( $D_0$ ) is twice the de Vaucouleurs radius. It ranges from  $< 1$  kpc for dwarfs to  $\sim 40$  kpc for large elliptical galaxies and is  $\sim 23.8$  kpc for Milky Way. It is 90 kpc for NGC 4489 (a D galaxy in the Coma cluster) and 220 kpc for A1153+23 (a cD galaxy in the cluster Abell 1413).

## 6.3 Spectrophotometric properties

There is a tight correlation of spectrum with Hubble type. Spectra vary from K giant for elliptical galaxies to A for Im (see Figure 6.2). Also, there is an increasing prominence of nebular emission lines, particularly  $H_\alpha$ , in later-type galaxies.

Multi-wavelength SEDs of galaxies are shown in Figure 6.3. The energy output peaks in the visible and far infrared (FIR). In the radio-FIR spectral range,  $F_\nu \propto \nu^{-\alpha}$  with  $\alpha \sim 2.3$ .

## 6.4 Star formation rate

The star formation rate (SFR) can be measured from the UV spectrum, which is dominated by young hot, stars. The best spectral region is around 125 nm, for which  $L_\nu(\nu)$  is nearly constant.

The Kennicutt relation (Kennicutt 1998) relates the star-formation rate to the UV luminosity,

$$SFR(M_\odot \text{ yr}^{-1}) = 1.4 \times 10^{-21} L_\nu(\text{ W Hz}^{-1}). \quad (6.5)$$

One can also estimate the SFR from nebular line strength (Kennicutt 1992)

$$SFR(M_\odot \text{ yr}^{-1}) = 7.9 \times 10^{-31} L_{H\alpha}(\text{ W}). \quad (6.6)$$

$$SFR(M_\odot \text{ yr}^{-1}) = (1.4 \pm 0.4) \times 10^{-21} L_{[OII]}(\text{ W}). \quad (6.7)$$

Equation (6.5) is the most accurate relation. The observed luminosities must be corrected for extinction both within the Milky Way and the target galaxy.

The star-formation rate can also be estimated from the far-infrared luminosity (FIR: 8 – 1000  $\mu\text{m}$ ). The connection occurs because radiation from young luminous stars is absorbed and

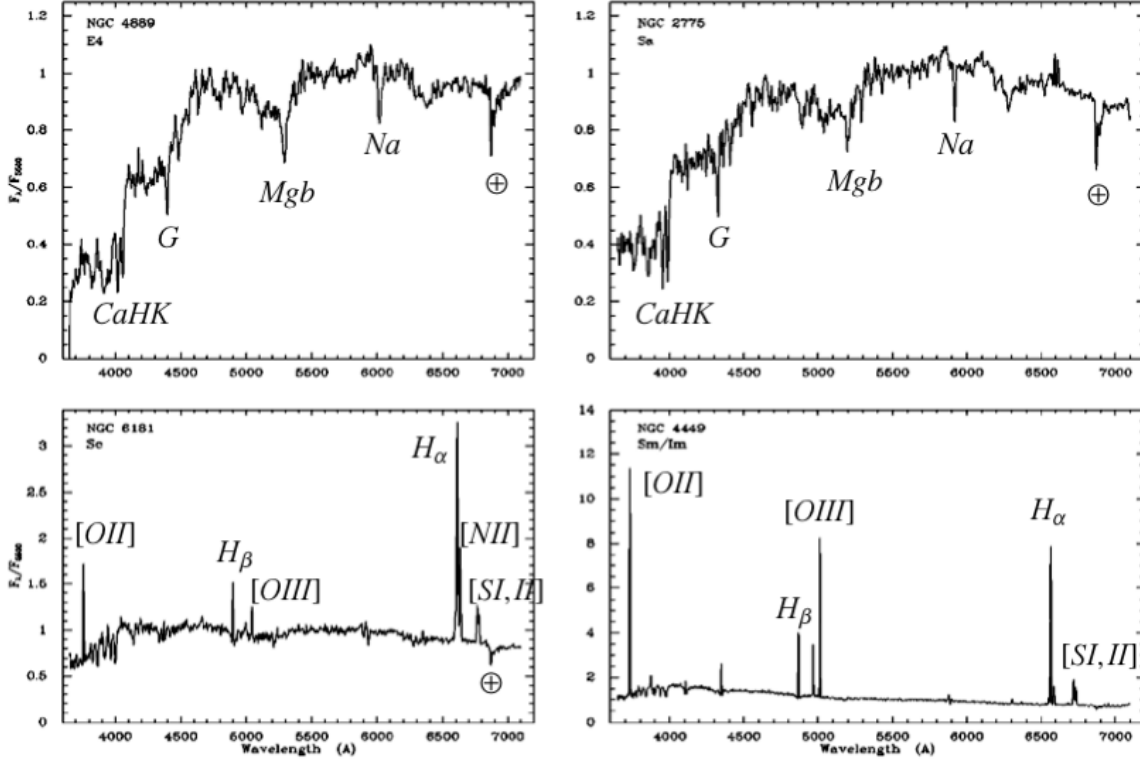


Figure 6.2: Spectral energy distributions of E, Sa, Sc and Im type galaxies. Note the flattening of the SED, due to increasing numbers of hot stars, and increasing prominence of emission lines (from Kennicutt 1998).

reradiated in the FIR by dust. If the dust opacity is high, as in starburst galaxies, the FIR luminosity reflects the SFR (Kennicutt 1998),

$$SFR(M_{\odot} \text{ yr}^{-1}) = 4.5 \times 10^{-37} L_{FIR}(\text{ W}). \quad (6.8)$$

Global star formation rates in normal galaxies range from 0 in E to  $\sim 20M_{\odot} \text{ yr}^{-1}$  in gas-rich spirals (Kennicutt 1998). Star formation rates as high as  $1000M_{\odot} \text{ yr}^{-1}$  are found in luminous starburst galaxies.

The star formation rate is found to correlate strongly with local gas density (Schmidt 1959, see Figure 6.4). The Schmidt law relates the star formation rate per unit area in the disk to the gas surface density,

$$\Sigma_{SFR} = (2.5 \pm 0.7) \times 10^{-4} \left( \frac{\Sigma_{gas}}{M_{\odot} \text{ pc}^{-2}} \right)^{1.4 \pm 0.15} M_{\odot} \text{ yr}^{-1} \text{ kpc}^{-2}. \quad (6.9)$$

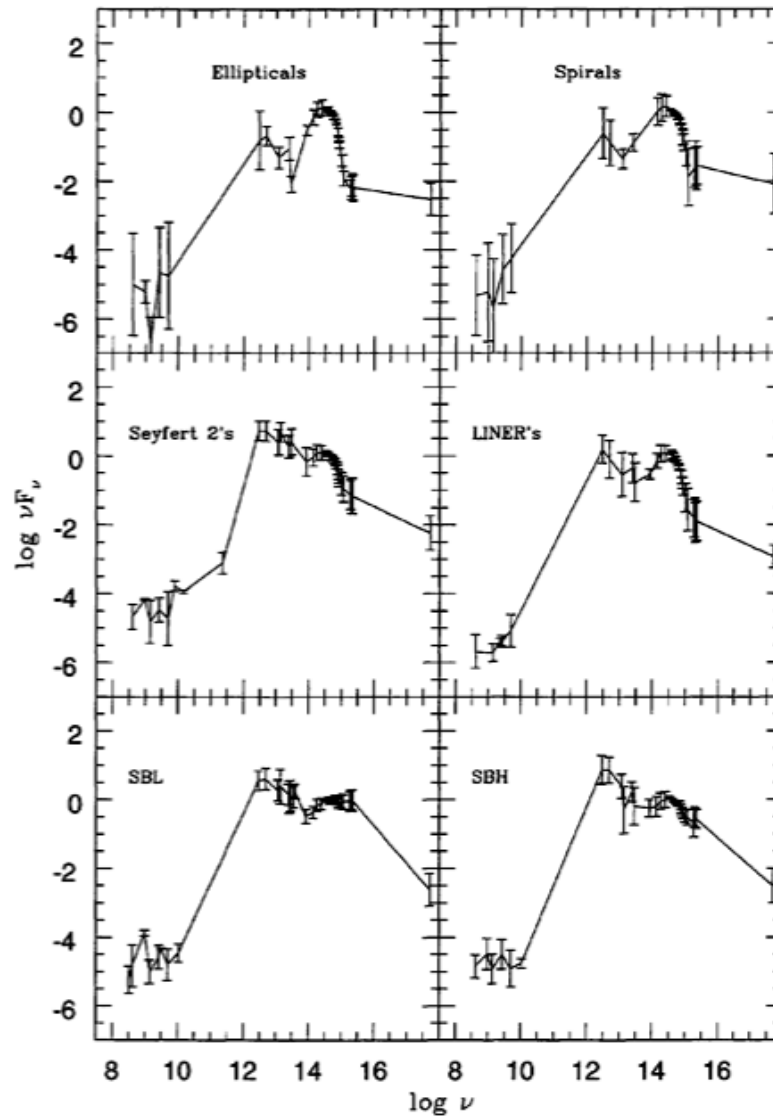


Figure 6.3: Multi-wavelength spectral energy distributions of galaxies. Normal elliptical and spiral galaxies are shown in the top two graphs (from Schmitt et al 1997).

## 6.5 Intrinsic shapes

Spiral galaxies seen edge-on give a direct indication of the intrinsic shapes of the disk and bulge.

The observed shapes of elliptical galaxies are related to the intrinsic shapes through (unknown) projection angles. However, from the statistics of large samples, one can in principle learn about the distribution of intrinsic shapes. For ellipsoids with rotational symmetry, viewed at

an angle  $\theta$  from the axis of symmetry, one has the following relationships between the intrinsic axial ratio  $\beta$  and the apparent axial ratio  $q$  :

$$q^2 = \begin{cases} \beta^2 \sin^2 \theta + \cos^2 \theta & \text{oblate,} \\ (\beta^2 \sin^2 \theta + \cos^2 \theta)^{-1} & \text{prolate.} \end{cases} \quad (6.10)$$

Assuming that galaxies are randomly oriented, this leads to the following integral equations relating the frequency functions of intrinsic and apparent axial ratios (Mihalas & Binney 1981)

$$f(q) = q \int_0^q \frac{N(\beta) d\beta}{\sqrt{(1-\beta^2)(q^2-\beta^2)}} \quad \text{oblate,} \quad (6.11)$$

$$f(q) = \frac{1}{q^2} \int_0^q \frac{N(\beta) \beta^2 d\beta}{\sqrt{(1-\beta^2)(q^2-\beta^2)}} \quad \text{prolate.} \quad (6.12)$$

Statistically, large elliptical galaxies are not well fit by prolate or oblate shapes, but require some degree of triaxiality (see Figure 6.5 and Figure 6.6).

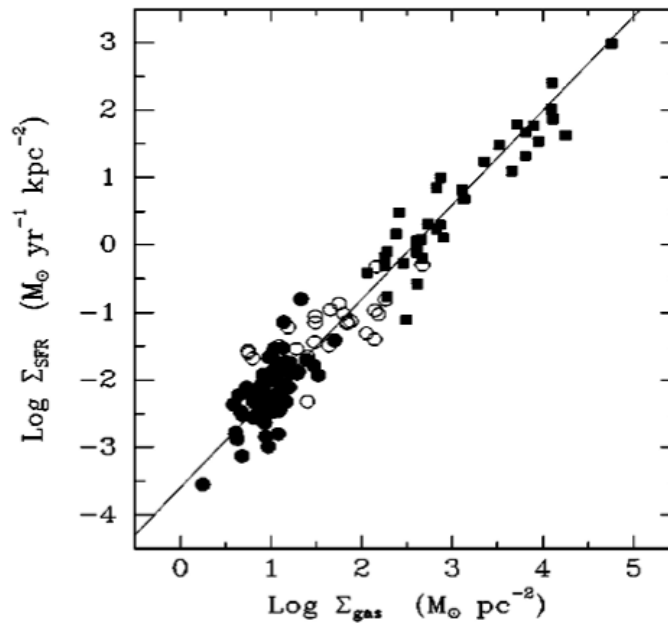


Figure 6.4: Global Schmidt law. Star formation rate correlates with local gas density over five orders of magnitude (from Kennicutt 1998).

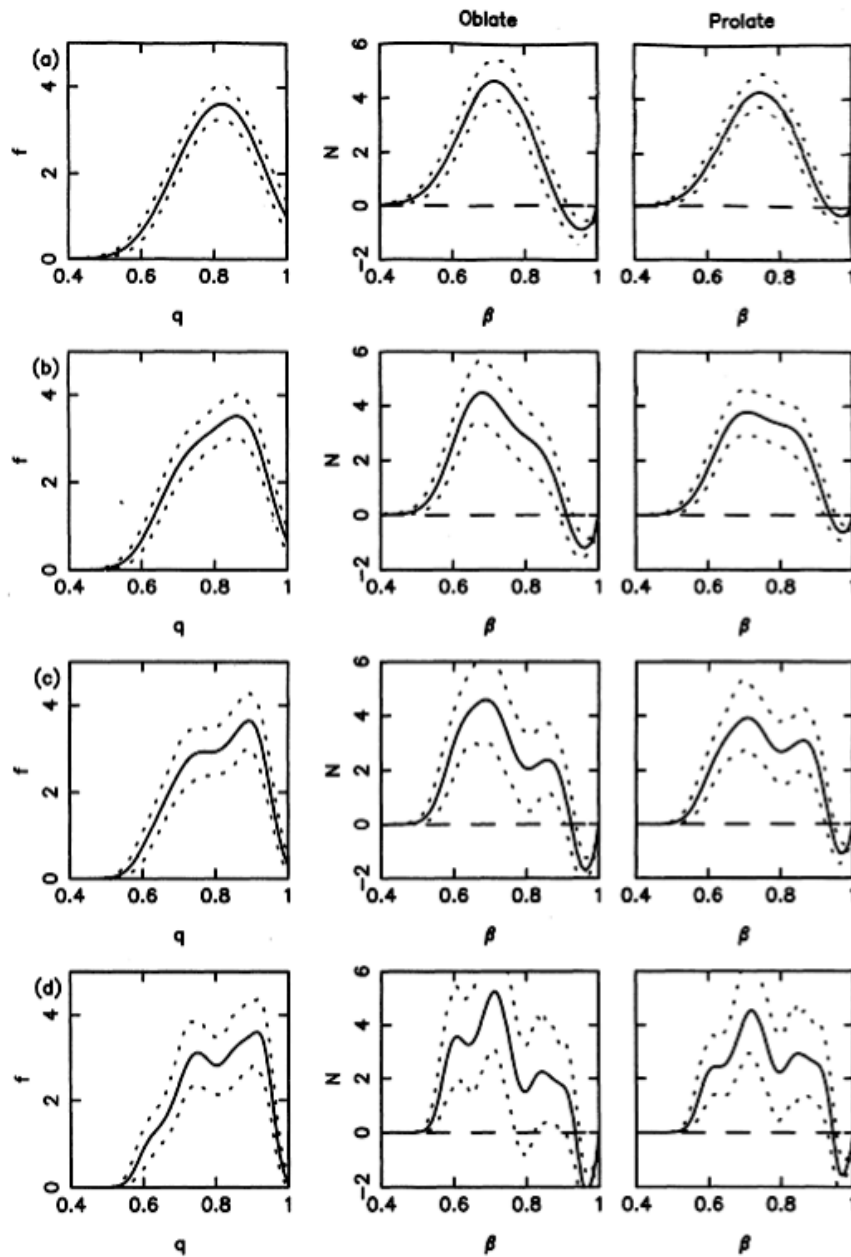


Figure 6.5: Distribution of observed axial ratios (left) with derived distributions of intrinsic axial ratios for oblate (centre) and prolate (right) spheroids. The rows (a) to (d) illustrate the effect of reducing the amount of smoothing applied to the observational data. Dashed lines denote 90% confidence intervals (Tremblay & Merritt 1995).

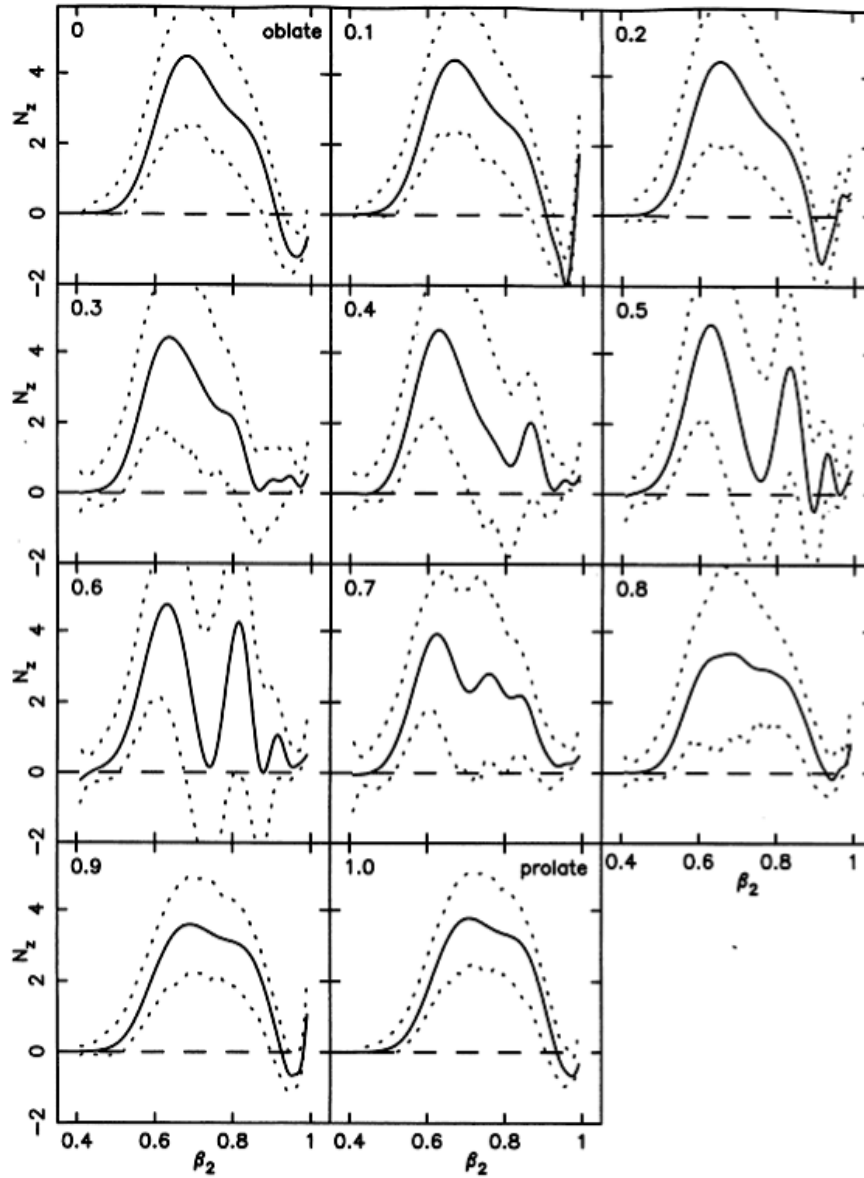


Figure 6.6: Derived distributions of intrinsic axial ratios for triaxial shapes. The number in the top left of each graph is the value of  $Z = (1 - \beta_1)(1 - \beta_2)$ . Satisfactory solutions exist for  $0.3 \leq Z \leq 0.8$  (Tremblay & Merritt 1995).